Image metrology and system controls for scanning beam interference lithography

Carl G. Chen,[a] Paul T. Konkola, Ralf K. Heilmann, G. S. Pati, and Mark L. Schattenburg
Massachusetts Institute of Technology, Cambridge, Massachusetts 02139

(Received 1 June 2001; accepted 16 August 2001)

We are developing scanning beam interference lithography (SBIL) for writing and reading large gratings with nanometer level distortion. Our distortion goals require fringe locking to a moving substrate with subnanometer spatial phase error while measuring and controlling the fringe period to approximately one part per million. In this article, we describe the SBIL optical system design along with some major subsystems. The design incorporates measurements and controls of the parameters that limit the accuracy of our system. We describe in detail a novel image metrology scheme, which uses interferometry to measure *in situ* both the period and the phase of the grating image formed by the interference of two laser beams. For a grating period of approximately 2 μm, experiments demonstrate a period measurement repeatability of three parts per ten thousand, one sigma. Phase measurement indicates a slow fringe drift at 0.25 mrad/s. Both the repeatability error and the phase drift are expected to improve by about three orders of magnitude after several improvements including the installation of an environmental enclosure and thermally stable metrology frames. [DOI: 10.1116/1.1409379]

I. INTRODUCTION

Interference lithography (IL) is the process of recording interference fringes. A good description of IL and its history is available elsewhere.[1] Figure 1 depicts our ''traditional'' IL system. Here, the pattern is defined by the interference of spherical waves. Shapes of the fringes produced by spherical waves have been studied in detail[1–4] and they contain an inherent hyperbolic distortion. The distortions limit the pattern size that can be considered linear.

In the traditional IL system (Fig. 1), the split beams are conditioned by several optics before interfering on the substrate. The variable attenuator equalizes the power of each of the interfered beams and thus maximizes fringe contrast. Polarizers may be included to ensure *s*-polarized light exposing the substrate. Spatial filters attenuate wavefront distortions by blocking undesired angular components of the beam. The focal length of the lens in the spatial filter is chosen to set the divergence of the beams, thereby defining the size of the region of interference. The beams typically have a Gaussian intensity distribution and the spot size on the substrate should be much larger than the desired interference pattern size for good dose uniformity. The distance from the spatial filter to the substrate defines the radius of the spherical wavefront. It is desirable for this distance to be large (typically >1 m) for reduced hyperbolic distortions. However, turbulence, vibration, and thermal drift limit the maximum practical propagation distance. Even with 1 m wavefront radii and the assumption of perfectly aligned beams, the image radius with subnanometer accumulated phase distortion is only 1.4 mm. This assumes a 400 nm nominal grating period produced with a 351.1 nm wavelength laser. Lenses may be used to collimate the beam after the spatial filter and thus eliminate the hyperbolic distortion. However, it is questionable as to whether it is practical to fabricate and align optics capable of producing large gratings with subnanometer fidelity.

A phase error sensor located near the plane of the substrate measures fringe drift, which is mainly due to air index changes, vibration, and thermal drift of the optical setup. The differential signal from two photodiodes is the error signal that drives the controller for a phase displacement actuator, which actuates so as to stabilize the fringes at the substrate. The nominal period, Λ, of the interference fringes is controlled by the beam incident angle θ and is given by

$$\Lambda = \frac{\lambda}{2 \sin \theta}. \tag{1}$$

Here, λ is the wavelength of the laser.

Despite the large hyperbolic distortions, interference lithography has many inherent advantages. First of all, the interference pattern produces highly coherent gratings. Secondly, the fringes have high contrast over a large depth of focus. Additionally, the topology of a spatial filter followed by no subsequent optics provides extremely low wavefront distortions. Other advantages include: built-in metrology of the interfered pattern,[1,3] a diffraction-limited resolution that is approximately twice that of traditional on-axis optical projection lithography, and excellent image contrast even at high numerical apertures.

II. SCANNING BEAM INTERFERENCE LITHOGRAPHY CONCEPT

The goal of the scanning beam interference lithography (SBIL) system is to write gratings and grids with subnanometer distortions over substrates up to 300 mm in diameter. These ultralow distortion gratings would enable important advances in metrology,[5] electro-optics, spectroscopy, and many other applications.

[a]Electronic mail: gangchen@mit.edu

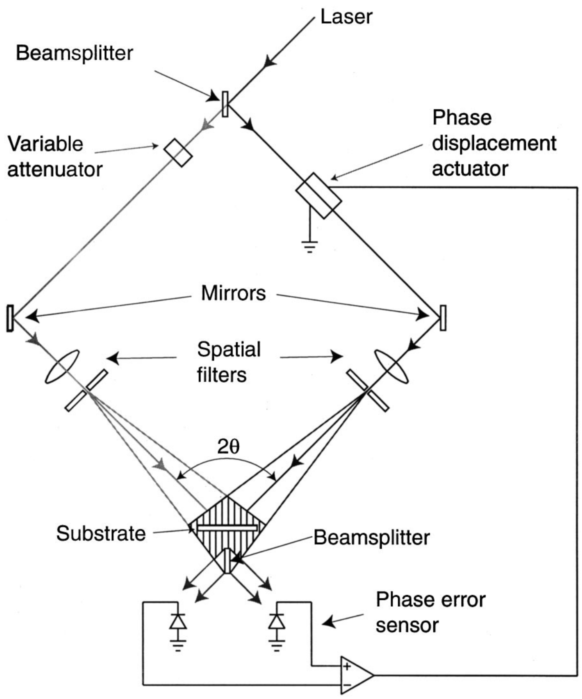

FIG. 1. Traditional IL system.

Figure 2 depicts the SBIL concept. The optics closely resemble those of the traditional IL system but the image is much smaller than the total desired patterning area. The grating image diameter is typically designed to be between 200 μm and 2 mm. Large gratings are fabricated by scanning the substrate at a constant velocity under the image. Figure 3 illustrates how SBIL achieves a uniform exposure dose by overlapping scans. Figure 3(a) shows the grating image being scanned along the substrate. At the end of the scan, the stage steps over by an integer number of grating periods and reverses direction for a new scan. The system has the significant added complexity over previous interference lithography systems of accurately synchronizing the interference image to the moving substrate. The scanning grating image is illustrated in Fig. 3(b). The interference pattern has a Gaussian intensity envelope since we interfere with Gaussian beams. The effective number of fringes in the scanning grating image may be many thousands (i.e., 10 000 fringes for a 2 mm $1/e^2$ image diameter and a 200 nm period grating). Figure 3(c) shows the individual scan intensity envelopes in dashed lines and the sum of the envelopes in the solid line. A maximum step size is constrained by the desired dose uniformity. For instance, a step size of 0.9 times the Gaussian beam $1/e^2$ radius produces dose uniformity of better than 1%.

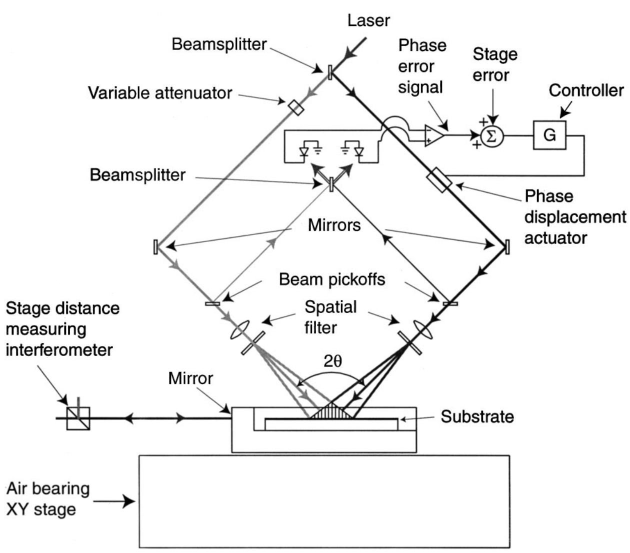

FIG. 2. SBIL concept.

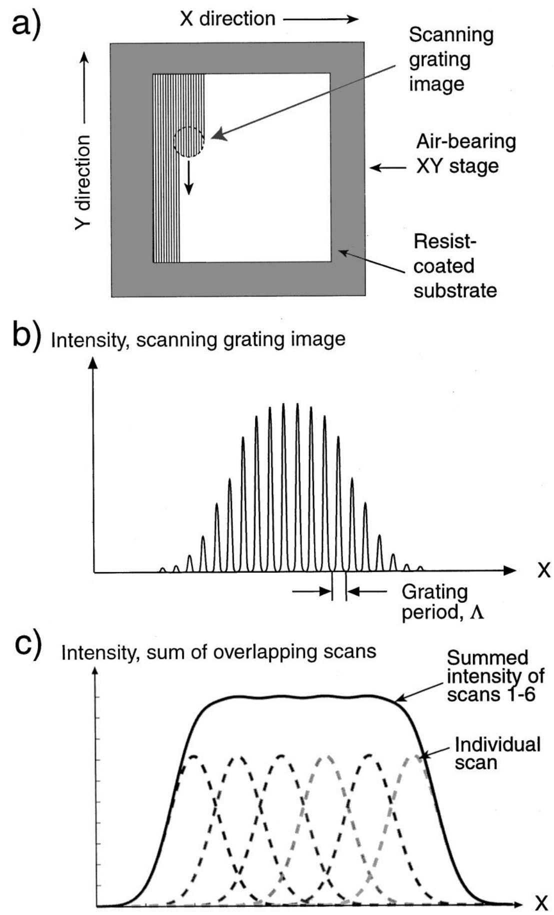

FIG. 3. Grating scan method.

Beam pick-offs direct a fraction of the power of each arm to a fringe locking system. The stage error and the lithography interferometer's signals are fed to the fringe locking controller, which in turn stabilizes the grating image in the reference frame of the moving substrate.

The relatively small beams used in SBIL provide a major benefit in ease of obtaining small wavefront distortions.[4] Furthermore, by scanning the image, distortions along the scan direction can be averaged out. The overlap of scans provides even further averaging of the wavefront distortions. Also, critical alignments, such as lens positioning and angle of interference, are much relaxed for the small beams.

In our approach, we aim to demonstrate repeatable grating

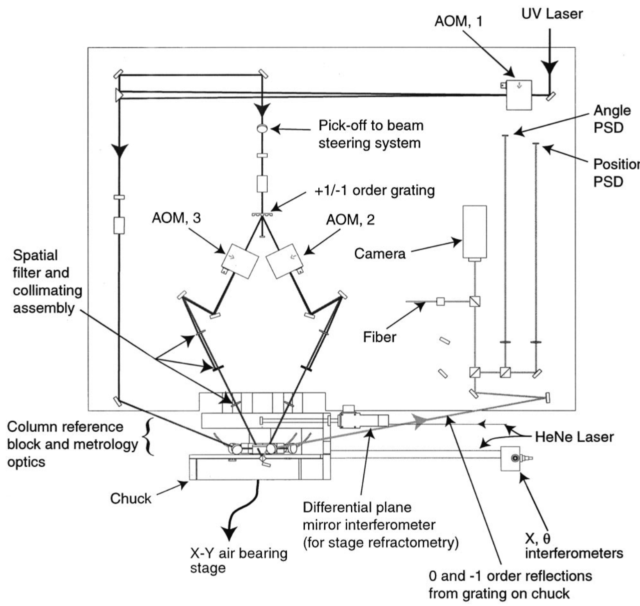

FIG. 4. SBIL system design.

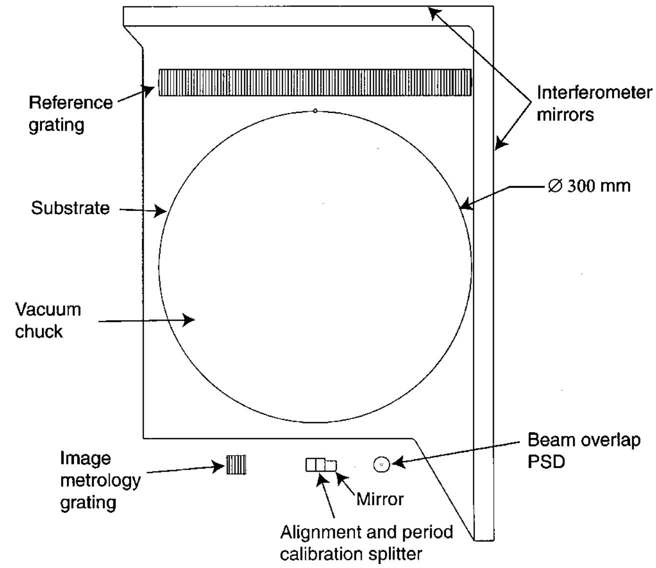

FIG. 5. Chuck with metrology references.

writing first. Then, self-calibration methods[6] will be implemented to correct systematic errors and finally achieve the accuracy goals. We are designing and implementing a system with a CW 351.1 nm wavelength argon–ion laser that is intended to achieve nanometer level distortions for arbitrarily selected grating periods in the range of 200 nm to 2 μm. Realizing our performance goals is a major challenge because of the many error sources in lithography. We categorize the errors for SBIL into five sources: non-plane wave, period control, substrate and metrology frame, displacement measuring interferometer, and lithography interferometer errors. The non-plane wave errors arise from the departure of the interfering wavefronts from planar. The period control errors are due to the writing period instability and period calibration inaccuracy. The substrate and metrology frame category refers to errors from substrate distortion and the inability of the metrology reference surfaces to accurately measure displacement between the fringes and the substrate. The interferometer categories refer to errors in the lithography and displacement interferometers. We describe the signals and controls in our system that are designed to measure and correct major error sources.

III. SBIL SYSTEM ARCHITECTURE

Figure 4 shows a simplified schematic of our optical system design along with some major subsystems. Details such as optical mounts are omitted. The system employs four column-referencing heterodyne interferometers to measure stage *x*- and *y*-axis displacement and yaw. Redundant yaw interferometry enables mapping of the stage systematic errors including stage mirror flatness and orthogonality. The design replaces the reflective beamsplitter of Fig. 2 with a $+1/-1$ order beamsplitter because it provides insensitivity to the spatial[7] and temporal coherence of the laser. The design includes a Class 10 environmental enclosure that provides acoustic attenuation and as well as controls over temperature (± 0.005 K), relative humidity ($< \pm 0.8\%$), and pressure gradient (<15.5 Pa/m). A differential-plane-mirror-interferometer-based refractometer corrects for environmentally induced index changes, which are mainly due to absolute pressure variations. Fringe drift and jitter in the optical bench are measured and corrected with a heterodyne phase measurement system and high-bandwidth acousto-optic fringe locking.[8] The fiber, column reference block, and metrology optics shown are part of this system. During scanning, a controller locks fringes in the reference frame of the moving substrate based on an error signal that incorporates stage position inaccuracy, index corrections, calibration data, and fringe drift measured in the metrology optics.

Figure 5 shows the chuck with metrology reference surfaces attached. Again, details such as optical mounts are omitted. The grating reference enables repeatable scale calibration of the stage interferometer that is substantially perpendicular to the grating lines. The grating is required to be about the same period that the system is set up to write and is read with a heterodyne fringe reading scheme.[8] The image metrology grating is a very high accuracy grating used to combine the reflected 0 and diffracted -1 order beams. A camera images the moiré pattern between the grating and the interference image, thus revealing small spatial frequency distortions. The moiré image also allows us to correct the radius of curvature of the interfering beams by repositioning the collimating lenses. The image metrology grating may be a small low-distortion patch of grating cut from a large grating fabricated by traditional IL. Alternatively, SBIL can produce this grating by overlapping many scans tightly, effectively averaging out the grating image nonlinearities.

The alignment and period calibration beamsplitter cube is used for *in situ* measurement of the period, phase, and rotation of the grating image, the first two of which we have demonstrated experimentally. Details will be presented in Sec. IV. An accurate period measurement enables the correct

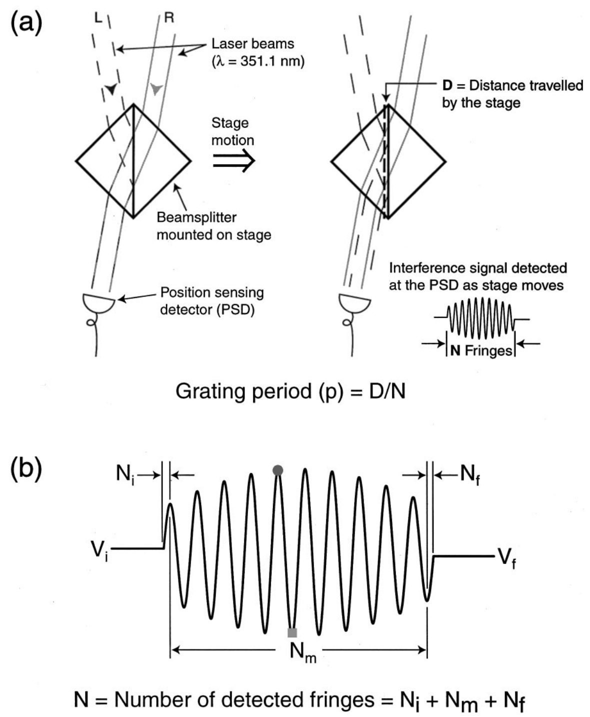

FIG. 6. (a) Image metrology via interferometry. (b) Fringe counting.

stitching of adjacent scans and makes a uniform, high-contrast exposure dose possible. Figure 6(a) shows the scheme. As the beamsplitter is laterally displaced, the optical path lengths for the left- and right-hand side beams will vary, leading to a sinusoidal intensity variation at a position sensing detector (PSD), whose power readout duplicates the intensity variation. The spatial period of the grating image can then be derived directly from this intensity readout. Furthermore, by moving the beamsplitter to a fixed location within the grating image and continuously sampling the power signal from the PSD, we can measure the grating phase at that location. During the writing or reading of a substrate, by periodically referencing the phase of the grating image to the beamsplitter, any slow drift in the optical system is detected, then compensated by adjusting the heterodyne fringe locking system. In principle, this phase referencing scheme is very similar to the automatic write scan correction method used in a MEBES electron beam writer, where the electron beam is periodically strobed over a reference grid in order to correct the scan length drift and the resulting stripe butting errors.[9]

The initial setup requires manual rough alignment of the interference angle θ. The period measurement system measures the actual image period and tunes the angles of interference by adjusting the appropriate picomotor-actuated mirror mounts. The optical design for the angle PSD and the position PSD decouples angle and position on the PSD's (Fig. 4). The PSD on the chuck (Fig. 5) is used to verify the beam overlap in the write plane and calibrate the decoupling matrices of the optical bench PSD's. It would be possible to use only the beam overlap PSD on the chuck and the angle PSD on the optical bench, but, this would require referencing the beamsplitter and the chuck PSD sequentially. The position PSD on the optical bench allows faster recalibration since only the beamsplitter on the chuck needs to be referenced. The faster calibration time reduces sensitivity to drift. Once the beam overlap and angles are calibrated, the system measures the optical power from the power reading provided by the overlap PSD. The beams are blankable by nulling the amplitudes of the rf signals to the acousto-optic modulators (AOM). The rf signal amplitudes to each AOM is adjusted to provide the same power from each beam to the substrate to the desired exposure dose.

Knowledge of the spot size on the substrate allows the accurate prediction of the dose and dose uniformity. The camera on the optical bench is also used for this measurement. Furthermore, the camera allows the imaging of the spot intensity distribution to ensure the beams have the intended Gaussian shape. Monitor wafers are typically written to establish optimal dose settings for a given resist.

During the grating reading, we can directly measure the fringe-to-grating motion with a phase interference measurement of the reflected zero-order and the diffracted first-order beams. This is important for determining the repeatability of the system and later for self-calibration procedures.

The electronic architecture is shown in Fig. 7. The real-time control platform contains a multiprocessor digital signal processing (DSP) board, D/A, A/D, interferometer, digital I/O, and digital change of state input cards. This platform controls the stage and fringe locking system as well as the overall patterning conditions. It communicates digitally with a LabView based computer that performs functions for period and phase measurement and alignment. The use of the two separate platforms allows parallel software and hardware development.

The system is designed to pattern a 300 mm diameter wafer in less than 7 min for the following conditions: 300 mm/s constant scan velocity, 0.25 g acceleration at the ends of the scans, a 2 mm beam diameter, and a sub-1% dose uniformity requirement. This is rapid compared to the state of the art in other direct write patterning technologies such as electron beam, ruling engine, or scanned laser writing. An active vibration isolation system with feed-forward is incorporated to allow fast settling times.

IV. IMAGE METROLOGY

SBIL is designed to create large area gratings with ultra-high phase linearity. Our ultimate design goal calls for sub-nanometer overall phase distortion across a 300 mm substrate when compared to a grating with an ideal linear phase. To enable the precise stitching of adjacent scans and to ensure a uniform, high-contrast exposure dose, our ability to determine the period of the grating image with extreme accuracy is critical. Formed by the interference of two narrow laser beams ($\lambda = 351.1$ nm), the grating image has a radius of 100 μm to 1 mm. Hence, to achieve 1 nm distortion at the edge of a 1 mm radius spot, we need to measure the period (p) to 1 nm/1 mm$=10^{-6}$, or one part per million, which translates to 2 pm for $p = 2$ μm and 0.2 pm for $p = 200$ nm.

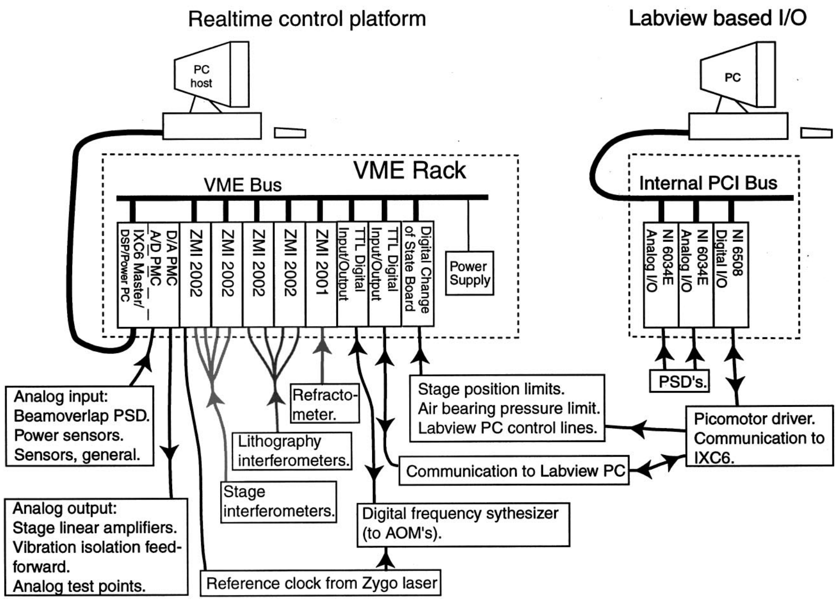

FIG. 7. SBIL system architecture.

Exposing the interference pattern in resist and measuring the period of the developed grating with a scanning electron microscope (SEM) is an extremely slow, laborious, and inaccurate process. Moreover, it yields period measurement in units traceable to the SEM used, whereas we desire length units defined by our particular displacement measuring interferometer (DMI), which is calibrated to a reference grating (Fig. 5). A direct aerial image measurement utilizing a slit artifact[10] is difficult to implement for small grating periods, due to energy throughput and fabrication reasons. We have thus developed a simple image metrology method using interferometry, which is capable of measuring the period of an aerial grating image in calibrated units within a few seconds and with high accuracy.

Figure 6 demonstrates our approach schematically. In the overlapping region of the two laser beams, we introduce a beamsplitter cube with its interface aligned parallel to the interference fringes. The beamsplitter is mounted on top of the air bearing stage, at a height approximately equal to that of the substrate. The reflected and the transmitted beams interfere and produce a signal at the power output of the PSD. Besides producing an intensity readout like an ordinary photodiode, a PSD is capable of providing an analog output directly proportional to the position of a light spot on the detector. As described earlier for the SBIL system architecture, we exploit this useful property to correctly set up and align the SBIL optics. As the stage moves, the optical path length difference between the two beams changes as well, leading to a sinusoidal intensity oscillation at the PSD. The intensity completes one cycle of oscillation as the stage traverses one fringe period. By dividing the stage travel distance by the total number of oscillations observed at the PSD, we can derive the period of the grating image.

The contrast of the intensity fringes at the PSD is maximum when the interfering beams are on top of each other, and decreases as the beams slide apart. The total number of fringes (N) is a sum of three terms: the fractional number of fringes N_i and N_f, and the integral number of fringes N_m, as illustrated in Fig. 6(b). A precise determination of N_i and N_f depends critically upon our knowledge of the initial and final signal levels, V_i and V_f, respectively. Furthermore, it rests upon our ability to unambiguously distinguish the peaks and valleys of the fringes. For the best resolution, V_i and V_f should be located close to points where the slopes of the fringes are steepest.

The stage-mounted beamsplitter can also be used for long-term drift compensation. Even with the best available environmental enclosure and metrology frames, it is likely that the SBIL system will experience minute thermal drifts over time. If uncorrected, these will result in the meandering of the grating lines and contribute to phase errors. Prior to the writing or reading of a grating, we place the beamsplitter to a location where the interference signal detected at the PSD has maximum contrast. The PSD power readout corresponds to the phase of the grating image at that particular location. For best phase resolution, it is also desirable to locate the grating phase at or near a zero-crossing. During the writing or reading, the beamsplitter is periodically returned to the same location and the phase sampled by the PSD. Any detected drift can then be compensated by the heterodyne fringe locking system.

V. METROLOGY RESULTS

54 sets of period measurements were carried out to test the repeatability of our measurement system, followed by a phase drift study. Throughout, the interference optics were set to produce a grating image period $p \approx 2$ μm, and the image was actively stabilized by an analog fringe locker. Other hardware included two On-Trak Photonics UV2L2 duolateral PSD's, one to ensure the precise overlap of the beam spots in the substrate plane and the other to sample the light intensity as described in the previous section. A/D conversion is handled by a National Instruments NI 6034E ana-

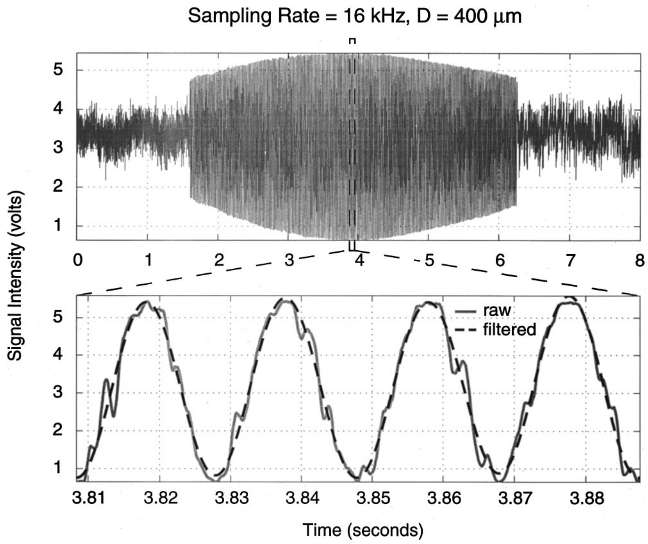

FIG. 8. Raw and digitally filtered period measurement data.

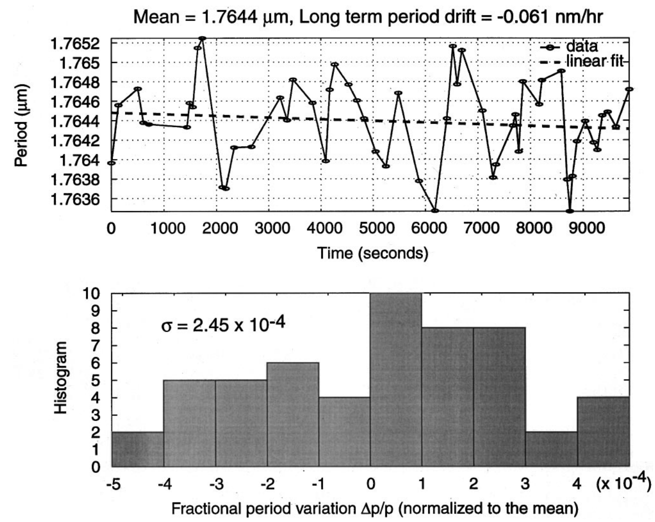

FIG. 9. Results of the period measurement repeatability.

log I/O board. The position sensing resolution of the PSD is limited by the resolution of the 16-bit I/O board to 31 nm, and its voltage resolution to 305.2 μV.

Figure 8 shows signals sampled at the PSD as the beamsplitter is displaced by an amount $D=400$ μm. The sample rate is at 16 kHz. A significant amount of noise is present. To implement a robust fringe counting algorithm, we must filter the data digitally. Power spectrum analysis reveals that the desired periodic signal is at 51 Hz. A finite impulse response (FIR) low-pass filter (with a Kaiser window) is then applied with a cutoff frequency at 70 Hz, a transition band width of 10 Hz and $\geqslant 60$ dB attenuation in the stop band. The filtered data is also shown in Fig. 8(b), with very well-defined peaks and valleys. A fringe counting algorithm was implemented in LabView, following the procedure outlined in the previous section. Signal levels V_i and V_f are calculated by averaging a large number of points (>8000) both at the beginning and at the end of the scan when the stage is at rest. Repeated measurements yield the repeatability results shown in Fig. 9. 54 separate measurements give the mean period at $p_{\text{mean}}=1.7644$ μm. The one-sigma $\Delta p/p$ repeatability is $\sigma=2.45\times10^{-4}$, or roughly three parts per ten thousand. A linear fit to the data indicates that the long term period drift was at 0.061 nm/h.

Following the period measurements, the beamsplitter cube was moved to a location where the signal at the PSD exhibited maximum contrast. The peaks and valleys were $V_p=5.4$ V and $V_v=0.7$ V, respectively, in the highest contrast region of the scan. A phase drift study was then carried out, lasting 45 min at a sample rate of 500 Hz. Figure 10(a) shows the power spectral density calculated from the data gathered. Significant noise power exists between 0.1 and 1 Hz, with a standard deviation $\sigma_{0.1\ \text{Hz}-1\ \text{Hz}}=0.28$ V_{rms}. These mid-frequency fluctuations contribute dominantly to the error in repeatability, as will be shown in the next section. Time domain data is plotted in Fig. 10(b), which reveals a long-term phase drift at 0.25 mrad/s. For better illustration, the data has been processed with a FIR low-pass filter with a cutoff frequency at 1 Hz, a transition band width of 0.2 Hz, and $\geqslant 60$ dB attenuation in the stop band.

VI. ERROR ANALYSIS AND DISCUSSION

We have demonstrated the use of interferometry to measure *in situ* the period and the phase of a grating image with $p\approx 2$ μm. A simplified best case model gives the following upper-bound error budget for $\Delta p/p=1$ nm/1 mm$=10^{-6}$:

$$\frac{\Delta V_i}{V_i}=\frac{\Delta V_f}{V_f}=1.3\times10^{-3} \quad \text{for } p=2\ \mu\text{m}, \tag{2}$$

$$\frac{\Delta V_i}{V_i}=\frac{\Delta V_f}{V_f}=1.3\times10^{-2} \quad \text{for } p=200\ \text{nm}, \tag{3}$$

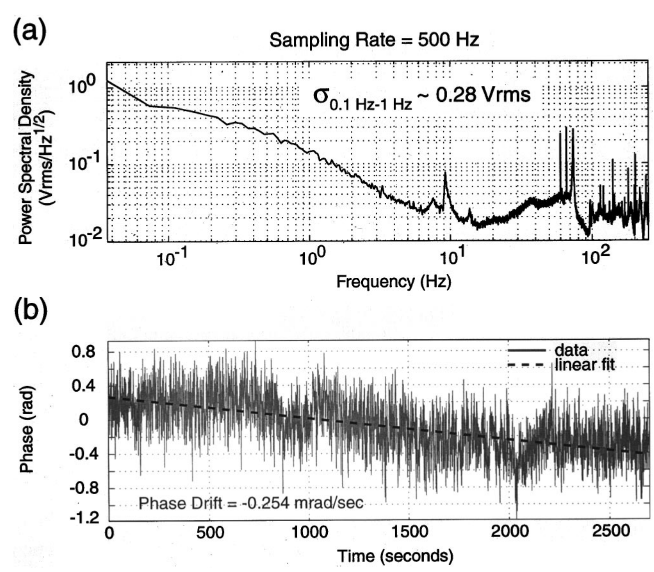

FIG. 10. (a) Power spectrum of the dc-subtracted phase data. (b) Phase data in time domain, processed with a low-pass filter with a cutoff at 1 Hz.

where we have assumed a stage displacement of 400 μm, a maximum fringe contrast $(\nu=(I_{\max}-I_{\min})/(I_{\max}+I_{\min})=1)$ and the existence of only high frequency voltage fluctuations. The required initial and final voltage resolution is ten times more stringent for a grating period $p=2$ μm than for $p=200$ nm. Intuitively, this makes sense. Given a fixed scan length, one can fit ten times more fringes at the shorter period, hence, the more relaxed specification. In practice, because of imperfect fringe contrast and multiple error budgets assigned to V_i, V_f, V_p, and V_v, the resolution must be higher.

Period measurement repeatability suffers from three main sources of error. They are best classified based on their behavior in the frequency domain: low frequency drift $(f \ll 0.1$ Hz), mid-frequency fluctuation (0.1 Hz$<f<$1 Hz) and high frequency fluctuation ($f \gg 1$ Hz). Low frequency drift due to thermal causes gives rise to the long-term phase drift, which is quantitatively measured in the previous section. At 0.25 mrad/s, the drift contributes an error $\sigma_{\text{low}} \approx 1\times10^{-6}$ towards the period resolution, for a measurement time of 10 s. While averaging a large number of data points to determine V_i and V_f can be very effective at getting rid of high frequency voltage fluctuations, it becomes less effective at mid frequencies. In fact, one can show that for our particular experiment, frequencies less than 1 Hz will pass through a moving average filter with length 5000. Since our period measurement lasts roughly 10 s, the lower limit of the mid-frequency interval is set at 0.1 Hz. We have already calculated the amount of mid-frequency noise between 0.1 Hz and 1 Hz, $\sigma_{0.1\text{ Hz}-1\text{ Hz}}=0.28$ V. In other words, for our experiment, V_i and V_f can be uncertain by an amount ± 0.28 V, which, when converted to period resolution error, gives rise to $\sigma_{\text{mid}} \approx 4\times10^{-4}$. Mid-frequency noise is most likely due to turbulence-induced air index change. Note that σ_{mid}, as calculated, represents only a lower limit for the mid-frequency noise, as we have ignored the effect of frequencies below 0.1 Hz. Nevertheless, it should provide a good order-of-magnitude estimate. Finally, at $f \gg 1$ Hz, we experience high frequency fluctuations, $\sigma_{\text{high}} \approx 2\times10^{-5}$, due to a combination of acoustic noise, stage and mechanical vibrations, and laser power fluctuations. Since the standard deviation of the mean decreases as $1/\sqrt{N}$, σ_{high} can be reduced further by averaging an even larger number of sampled data points.

What we have just presented is only an order-of-magnitude calculation. However, $\sigma_{\text{tot}}=\sqrt{\sigma_{\text{low}}^2+\sigma_{\text{mid}}^2+\sigma_{\text{high}}^2} \approx 4\times10^{-4}$ corresponds to the measured value $\sigma=2.45\times10^{-4}$ very well. The error analysis suggests that mid-frequency noise is by far the most dominant error source. It should be noted that our experiments have been performed without the use of an environmental enclosure or properly designed low coefficient of thermal expansion (CTE) metrology frames. Even though an active fringe stabilization system is used, the stabilizing action does not strictly take place at the location of the grating image since it is impractical to implement. Any relative optical path length change from the grating image to the point of actual fringe locking may introduce phase jitters.

Soon, the SBIL system will undergo a major upgrade. The additions of an environmental enclosure and low CTE metrology frames, together with a more compact fringe locking system, will significantly reduce the repeatability error and the long term phase drift. Furthermore, it is possible to reduce the mid-frequency noise by considerably boosting the stage scan speed and the data sampling rate. This relies on the establishment of a seamless communication protocol between our LabView based data I/O and the real-time control platform (Fig. 7), a process that we have started to work on.

VII. CONCLUSIONS

We have described the design for SBIL. The design incorporates measurements and controls of the parameters that limit the accuracy of our system. We have also described in detail a novel image metrology scheme, which uses interferometry to measure *in situ* both the period and the phase of a grating image formed by the interference of two laser beams. Measurement data is presented and different error sources analyzed. Correctly addressing the many error sources in lithography should ultimately allow the patterning of gratings and grids with subnanometer distortions over a 300 mm substrate.

ACKNOWLEDGMENTS

The authors gratefully acknowledge the outstanding technical assistance of Robert Fleming and Edward Murphy. Student, staff, and facility supports from the Space Nanotechnology Laboratory and the NanoStructures Laboratory are also appreciated. This work was supported by DARPA under Grant No. DAAG55-98-1-0130 and NASA under Grant No. NAG5-5271.

[1] J. Ferrera, Ph.D. dissertation, Massachusetts Institute of Technology, 2000.
[2] K. Hibinio and Z. Hegedus, Appl. Opt. **33**, 2553 (1994).
[3] J. Ferrera, M. Schattenburg, and H. Smith, J. Vac. Sci. Technol. B **14**, 4009 (1996).
[4] C. G. Chen, M.S. thesis, Massachusetts Institute of Technology, 2000.
[5] M. Schattenburg *et al.*, J. Vac. Sci. Technol. B **17**, 2692 (1999).
[6] C. J. Evans, R. J. Hocken, and W. T. Estler, CIRP Ann. **45**, 617 (1996).
[7] P. Konkola, C. G. Chen, R. Heilmann, and M. L. Schattenburg, J. Vac. Sci. Technol. B **18**, 3282 (2000).
[8] R. K. Heilmann *et al.*, J. Vac. Sci. Technol. B, these proceedings.
[9] H. Pearce-Percy *et al.*, J. Vac. Sci. Technol. B **12**, 3393 (1994).
[10] W. N. Partlo, C. H. Fields, and W. G. Oldham, J. Vac. Sci. Technol. B **11**, 2686 (1993).